CO_2 laser with modulated losses: Theoretical models and experiments in the chaotic regime

C. L. Pando L.
International Center for Theoretical Physics (I.C.T.P.), Strada Costiera 11, P.O. Box 586, Trieste, Italy

R. Meucci, M. Ciofini, and F. T. Arecchi
Istituto Nazionale di Ottica, Largo E. Fermi 6, 50125 Firenze, Italy

We compare two different theoretical models for a CO_2 laser, namely, the two- and four-level model, and show that the second one traces with much better accuracy the experimentally observed chaotic dynamics when the cavity losses are sinusoidally modulated. Even though the two-level model provides a qualitative explanation of the chaotic dynamics, only the four-level one assures a quantitative fitting. We also show that, at the onset of chaos, the chaotic dynamics is low dimensional and can be described in terms of a noninvertible one-dimensional map.

I. INTRODUCTION

A loss modulated single mode CO_2 laser was the first optical device for which chaotic dynamics were investigated in a detailed way. The evidence of chaos was not limited to irregular time patterns or broadened power spectra, but was provided by quantitative characterizations of the chaotic scenario by suitable indicators.[1] At the same time, considerable effort has been invested to provide the simplest exhaustive theoretical model for the CO_2 laser able to reproduce adequately the experiments.[2–5] The widely used approach based on two rate equations for the photon number n and the population inversion δ (Ref. 1) (two-level model, 2LM) provides only a qualitative agreement with the experiments. In a recent paper[5] it has been shown that in a Q-switch experiment the main limitations of 2LM appear when the amplification regime is not linear and saturation effects induced by the coupling between n and δ become relevant. More accurate results can be obtained by using the so-called four-level model (4LM) which takes into account the collisional coupling of each resonant energy level with a certain number of rotational levels of the same vibrational band.

The aim of this paper is to extend the analysis of Ref. 5 comparing the two different models with an experimental situation where nonlinearities play a fundamental role, that is, when chaotic dynamics are obtained by modulating the cavity losses. The parameter values used here are the same as those of Ref. 5, which, on the one hand provide a satisfactory agreement with Q-switching experiments, and on the other are close to those of previous studies.[2,3]

In order to make a more complete comparison, we have considered two cases of 2LM. In the first (two-level model standard, or 2LMS) the value of the population decay rate γ to be considered in the rate equations is in the range of the values measured directly by spectroscopic techniques. As a consequence, no agreement is reached between the measured and calculated saturation intensities. To account for this, a second model (two-level model equivalent, or 2LME) is considered, for which the value of γ is derived by the requirement that the predicted value of saturation intensity should agree with the experimental one, and this requires a value of γ that is much higher (by an order of magnitude) than the actual value.

Trying to fit all the experimental features of the chaotic dynamics with theoretical predictions, we will show that both two-level models give unrealistic results while the four-level model describes with a good degree of accuracy the experiment. 2LMS shows chaotic evolution for a range of modulation frequencies close to the experimental value but for much lower modulation amplitudes, while 2LME provides chaos for the correct range of modulation amplitudes but for higher modulation frequencies. 4LM is free of both drawbacks.

Besides the comparison between the theoretical models and the experimental results, we have investigated two experimental features that had received little attention before, namely, the collapse of two Feigenbaum cascades[6] and the one-dimensional-map contraction of the laser dynamics at the onset of chaos.[7] In fact it was the analysis of 4LM which stimulated us to search for these experimental properties, which in turn are related with one another.[8,9] We find a type of behavior in our system involving a sequence of period doublings followed by the inverse process as the modulation amplitude is kept constant and the modulation frequency is varied. Following Ref. 6 we call this behavior "period bubbling." Depending on the strength of the modulation amplitude the sequence of period doublings may not reach chaos giving rise in this way to a big primary bubble within which higher-order bubbles are contained.[9] Such a behavior has been found in other systems[8] and seems characteristic of low-dimensional dynamics. The other experimental feature, that is, the one-dimensional map behavior, is expected as a consequence of a sequence of subharmonic bifurcations. This general result has been demonstrated by renormalization group analysis in multidimensional systems.[7] However, these features do not appear for all parameter values since crises may take place.[10,11] Let us point out that generalized multistability found in lasers[1] is related to the existence of crises of the attractor destruction type, since it suggests the coexistence of different attractors. In other words, multistability may inhibit period bubbling behavior.

The paper is divided as follows. Section II concerns the

 1054-1500/93/3(3)/279/7/$6.00

TABLE I. Experimental bifurcation values of the parameters V_1 and $m=m_e$ for $f=100$ kHz; m_t is the corresponding theoretical value for the 4LM. The uncertainty on V_1 is ± 1 V.

V_1 (V)	m_e	m_t	onset of
31	0.046	0.047	$f/2$
72	0.106	0.082	$f/4$
78	0.115	0.098	$f/8$
84	0.124	0.105	chaotic $f/2$
104	0.153	0.152	chaotic $f/3$

description of the experimental setup. In Sec. III we describe the theoretical models and compare them with the experimental results. In Sec. IV we give the conclusions.

II. EXPERIMENTAL SETUP AND RESULTS

The experimental measurements have been performed with a laser cavity defined by a grating and a 90% reflectivity mirror with a radius of curvature of 3 m placed 1.35 m apart. Single mode operation is achieved by means of an intracavity diaphragm. The laser is operated with a gas mixture of $CO_2 \simeq 9\%$ vol., $N_2 \simeq 12\%$ vol., and $He \simeq 79\%$ vol., at a total pressure of 20 Torr, flowing in a Pyrex tube with 10 mm of internal diameter. The active medium excitation is obtained via a current stabilized longitudinal dc discharge at a fixed current value of 5.0 mA.

An intracavity electro-optic modulator (EOM) modulates the intracavity field transmission so that the cavity damping rate can be expressed as follows:

$$K=\frac{c}{2L}\left[2T+(1-2T)\sin^2\left(\frac{\pi V(t)}{V_\lambda}\right)\right], \tag{1}$$

where c is the speed of light, L is the cavity length, $T=0.10$ is the total transmission coefficient for a single pass, $V_\lambda=4240$ V, and $V(t)=V_0+V_1\sin(2\pi ft)$ is the voltage applied to the EOM ($V_0=700$ V). Considering that $V(t)\ll V_\lambda$ we can approximate the expression for K as

$$\begin{aligned} &K=k[1+m\sin(2\pi ft)], \\ &k=\frac{c}{2L}\left[2T+(1-2T)\left(\frac{\pi V_0}{V_\lambda}\right)^2\right], \\ &m=\frac{2V_1}{V_0}\frac{1}{1+\alpha}, \\ &\alpha=\frac{2T}{1-2T}\left(\frac{V_\lambda}{\pi V_0}\right)^2, \end{aligned} \tag{2}$$

where k represents the cavity damping rate when the modulation amplitude m is set to zero [$k=4.61\times10^7$ s^{-1} from Eqs. (2)].

Working with a fixed modulation frequency, we have increased the modulation amplitude m by changing V_1. The subharmonic cascade in the laser signal leading to chaos has been characterized by measuring the values of the control parameter V_1 at which successive bifurcations occur (see Table I). We have recorded three bifurcation sequences at $f_1=90$ kHz, $f_2=100$ kHz, and $f_3=110$ kHz.

TABLE II. Experimental bifurcation values of the parameter f for $V_1=73.5$ V corresponding to $m=0.108$ (the uncertainty on f is $\simeq 1$ kHz).

f	$f/2$	$f/4$	$f/2$	f	
46	96	118	151		f(kHz)

At $f=f_2$ we have also recorded stroboscopic Poincaré sections of the laser output intensity each with 64 000 periods.

In addition, by changing the modulation frequency f at a fixed value of m, we have characterized the period-bubbling phenomenon. The result of the measurement is reported in Table II.

III. THEORETICAL MODELS AND COMPARISON WITH EXPERIMENTS

If we consider the CO_2 molecule as a simple two-level system coupled with a resonant electric field, we can describe the laser dynamics (in the case of sinusoidal loss modulation) with two differential equations for the photon number n and the population inversion δ between the two resonant levels (2LM) (dot denotes the time derivative):

$$\begin{aligned} &\dot n=kn\{\delta-[1+m\sin(2\pi ft+\phi)]\}, \\ &\dot\delta=-\gamma\delta-2kn\delta+\gamma GP/k. \end{aligned} \tag{3}$$

When $m=0$, n and δ have been renormalized to the steady state inversion, γ is the inversion decay rate [for the 2LMS $\gamma=1.95\times10^4$ s^{-1}, for 2LME $\gamma=1.95\times10^5$ s^{-1} (Ref. 5)], $G=9.9\times10^{-8}$ s^{-1} is the field-matter coupling constant, $P=6.64\times10^{14}$ is the pump parameter, and ϕ is the phase shift. Values of G and P are rescaled from those given in Ref. 5.

As a matter of fact, the above description does not take into account the collisional coupling of each resonant level with a certain number Z of rotational levels of the same vibrational band (detailed physical considerations and the relevant energy level diagrams are reported in Refs. 2–5). The introduction of such a coupling leads to a set of five differential equations (4LM) for the photon number n, the population inversion δ and the population sum σ of the resonant levels, and the population inversion Δ and the population sum Σ of the rotational manifolds:

$$\begin{aligned} &\dot n=kn\{\delta-[1+m\sin(2\pi ft+\phi)]\}, \\ &\dot\delta=-\Gamma\delta+\gamma\sigma+\gamma_R'\Delta-2kn\delta+\gamma_2GP/k, \\ &\dot\sigma=-\Gamma\sigma+\gamma\delta+\gamma_R'\Sigma+\gamma_2GP/k, \\ &\dot\Delta=-\Gamma'\Delta+\gamma\Sigma+\gamma_R\delta+\gamma_2GZP/k, \\ &\dot\Sigma=-\Gamma'\Sigma+\gamma\Delta+\gamma_R\sigma+\gamma_2GZP/k. \end{aligned} \tag{4}$$

All the variables have been rescaled to the steady-state inversion of the resonant levels when $m=0$. The number of rotational levels considered in each manifold is $Z=10$. The decay rates Γ, Γ', and γ are defined as follows:

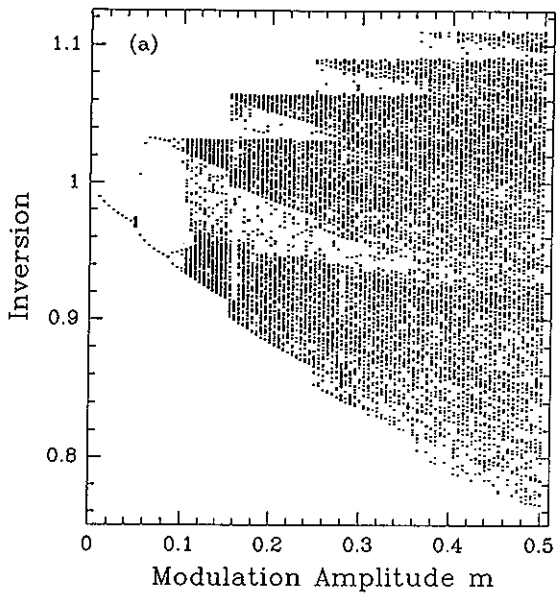

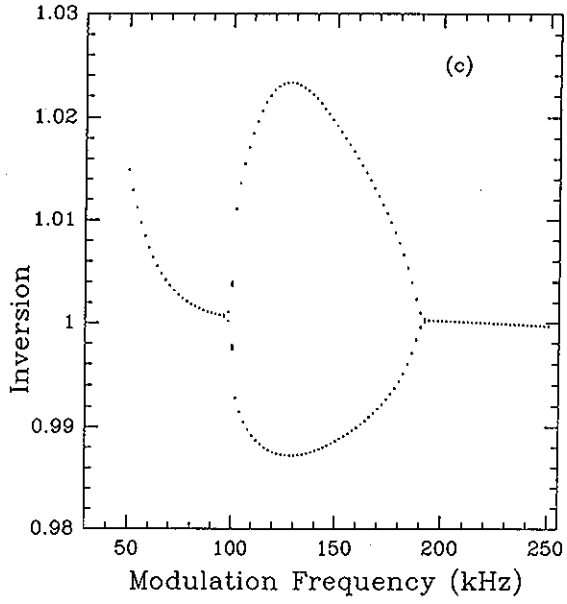

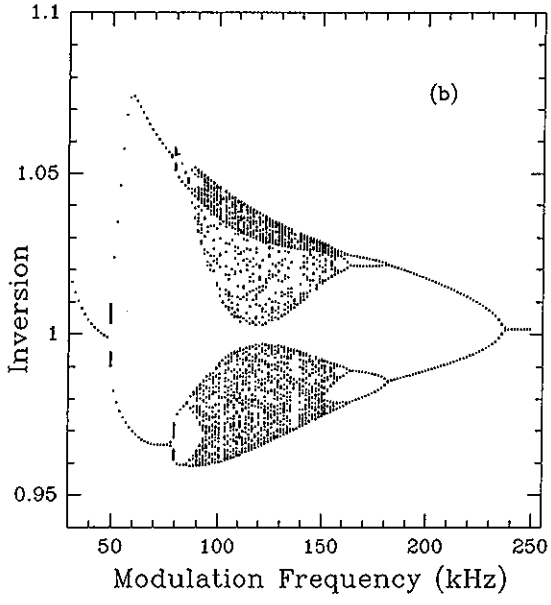

FIG. 1. Numerical results for 4LM. (a) Bifurcation diagram for the inversion δ versus the modulation amplitude m at $f=100$ kHz. (b) Bifurcation diagram of δ versus the modulation frequency f at $m=0.11$. (c) The same as (b) but for $m=0.05$.

$$\Gamma=(\gamma_1+\gamma_2)/2+\gamma_R,$$
$$\Gamma'=(\gamma_1+\gamma_2)/2+\gamma_R', \quad (5)$$
$$\gamma=(\gamma_1-\gamma_2)/2,$$

where $\gamma_R=7.0\times10^6\,s^{-1}$, $\gamma_R'=7.0\times10^5\,s^{-1}$, $\gamma_1=8.0\times10^4\,s^{-1}$, and $\gamma_2=1.0\times10^4\,s^{-1}$ (according to Refs. 2 and 5). The other parameters are the same as in the two-level model.

In what follows we will compare the two- and the four-level models with the experimental results of the previous section by using bifurcation diagram analysis. Once we show that the four-level model is the most suitable one, we further study it in terms of Poincaré sections and return maps.

In Fig. 1(a) we report the bifurcation diagram for 4LM at a fixed value of the modulation frequency $f=100$ kHz. In Fig. 1(b) we report the bifurcation diagram at a fixed value of the modulation amplitude $m=0.11$. For this value of m the subharmonic window is bounded between 50 and 200 kHz. In Fig. 1(c) we report the primary bubble in 4LM at $m=0.05$ as the frequency is scanned. It can be verified from these figures and from Table I that the numerical results are in agreement with the experiment (the same agreement has been found at $f=90$ and 110 kHz).

In Fig. 2(a) we report the bifurcation diagram for 2LME at a fixed modulation frequency $f=100$ kHz. Comparing Figs. 1(a) and 2(a) we observe that 4LM is more easily destabilized than 2LME. As we may see in 4LM [Fig. 1(a)] upon change of m, after the first continuous chaotic region a new chaotic attractor is originated from a period-3 unstable orbit. This crisis also occurs for $m\approx0.15$ upon change of f and the attractor may be periodic or chaotic depending on f. A similar situation occurs for 2LME but for unphysical values of the parameters m and f. Figure 2(b) shows that, for the modulation amplitude $m=0.11$, the subharmonic region is shifted to frequencies higher than 120 kHz. 2LME also shows period bubbling for small values of m (≈0.05).

As regards 2LMS, the bifurcation diagram at $f=100$

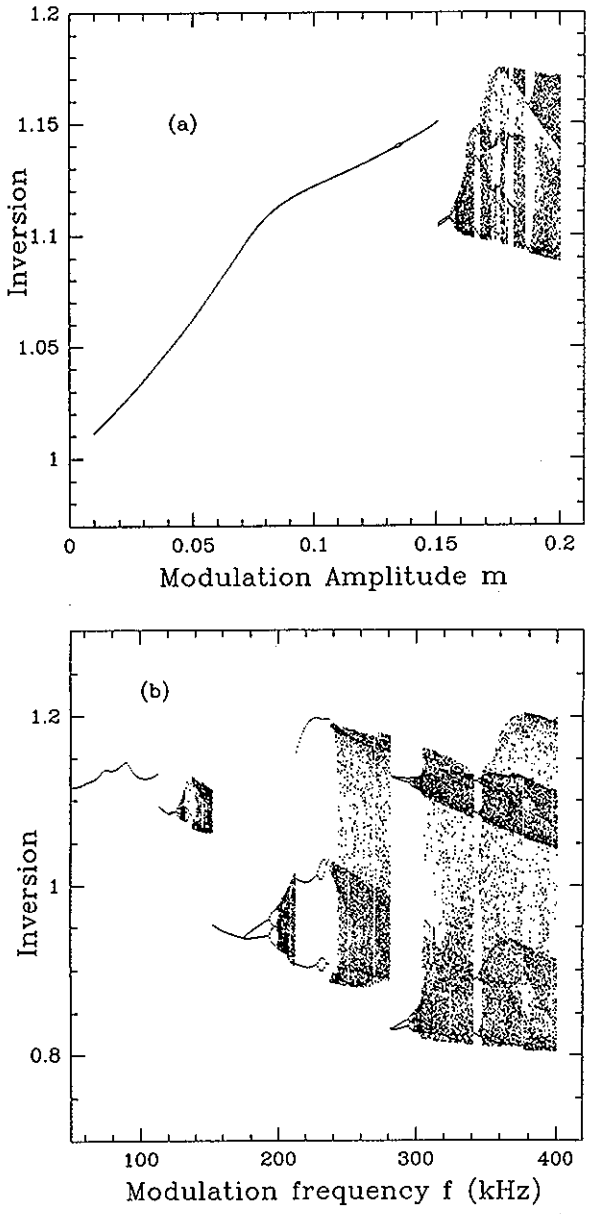

FIG. 2. Numerical results for 2LME. (a) Bifurcation diagram of δ vs m at $f=100$ kHz. (b) Bifurcation diagram for the inversion δ versus the modulation frequency at $m=0.11$.

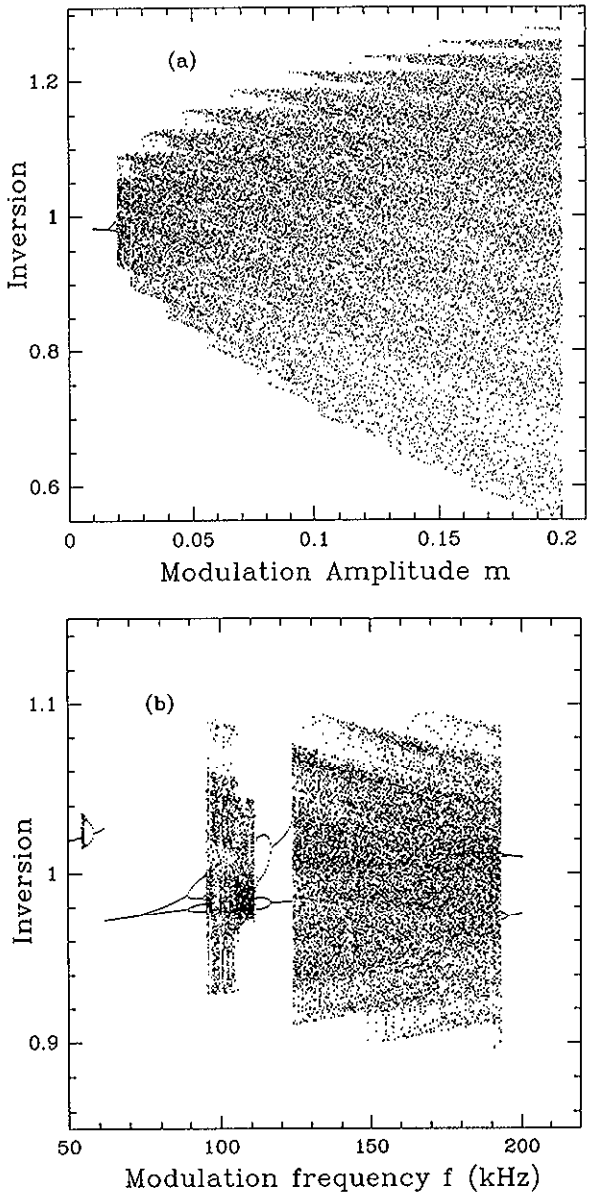

FIG. 3. Numerical results for 2LMS. (a) Bifurcation diagram of δ vs m at $f=100$ kHz. (a) Bifurcation diagram for the inversion δ versus the modulation frequency at $m=0.02$.

kHz reported in Fig. 3(a) shows a continuous chaotic region which resembles roughly the bifurcation diagram of 4LM. The general difference is that successive crises in 2LMS are separated by small intervals of m in comparison with those of 4LM. In Fig. 3(b) we see that for $m=0.02$ 2LMS not only predicts chaos but also several crises as the frequency is scanned. The interval of modulation frequencies where the subharmonics occur is roughly the same as in 4LM for small values of m, but period bubbling is not allowed due to the collision of the attractor (periodic orbit) with its basin boundary.

Comparing the numerical results of different models we can see that both the two-level models present relevant discrepancies with respect to 4LM. The main problem of 2LMS is the onset of chaos at low values of the modulation amplitude m.[1] One may think to improve this matter by increasing the decay rate γ thus increasing the value of m required to reach the chaotic regime. However, as we have seen in 2LME, the price that one pays is that the frequency region where subharmonics appear is shifted far from that of the experiment. We have found these features also with the parameter set reported in Ref. 5.

We now compare the experimental Poincaré sections at the onset of chaos with those of the numerical simulations of 4LM. The projections of the numerical Poincaré section for period four in the plane (n,n) is shown in Fig. 4. Here we marked the order of the successive iterations. Figure 5 shows similar Poincaré sections at the onset of the chaotic regime ($m=0.105$ and $f=100$ kHz). Figure 4 suggests that the attractor represented in Fig. 5 consists of four pieces, which are visited in sequence. In fact, if we make a map by sampling the intensity or the inversion

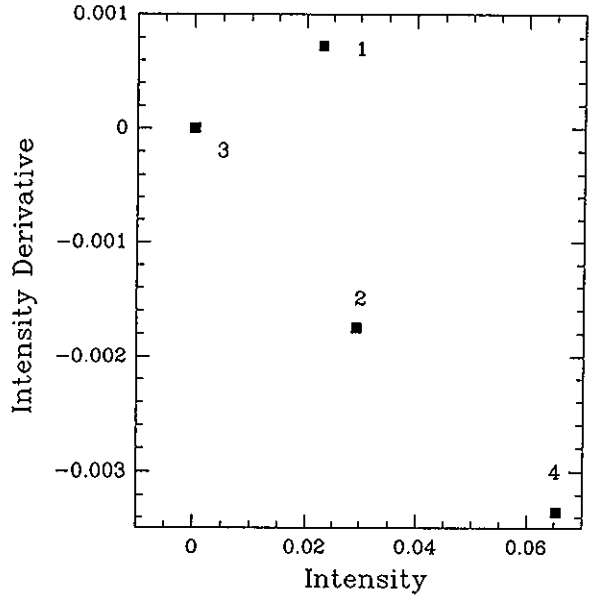

FIG. 4. Numerical Poincaré map projection of the intensity derivative ($\dot{n}$) versus the intensity (n) at $f=100$ kHz and $m=0.09$ (period four).

every four periods, we will find four different return maps.

As we may see in Fig. 5 a common feature of the return map is that a Cantor set structure (related to the horseshoe dynamics of the equations) occurs on a very fine scale and therefore an effective one-dimensional map may represent the dynamics of the equations.

Two of the pieces of the map reported in Fig. 5 show a one-to-one correspondence between the points of the vertical and horizontal axes. Thus we construct the return map whenever the orbit is localized in one of these pieces, i.e., we form a one-dimensional map by sampling the intensity or the intensity derivative every fourth iterate of the

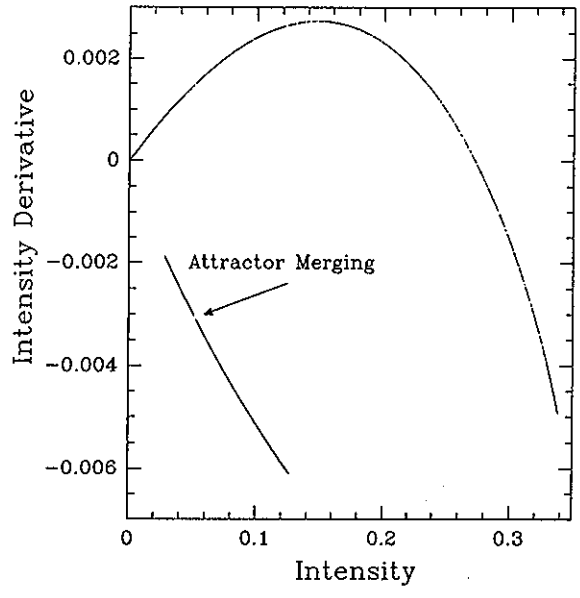

FIG. 5. The same as Fig. 4 but for $m=0.105$ (onset of chaos). The attractor merging of the "linear" pieces is shown (it is also observed in the other two pieces).

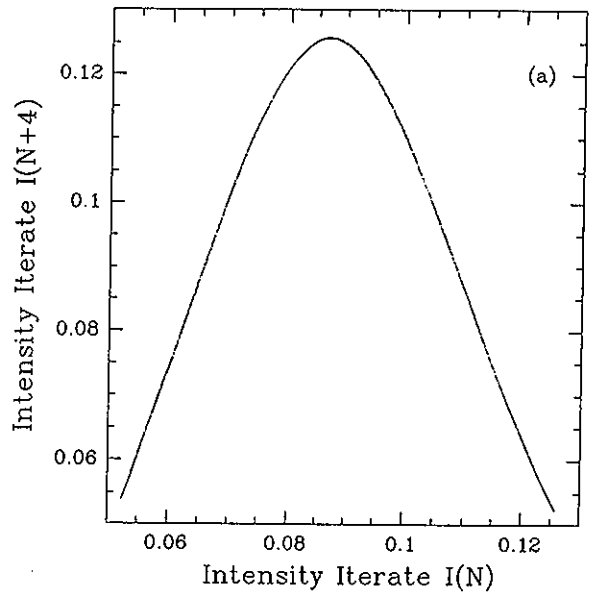

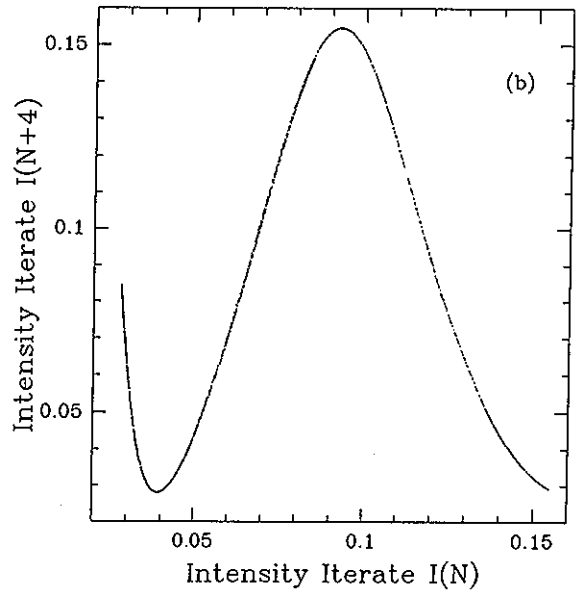

FIG. 6. Numerical return maps obtained with the fourth iterates of the photon number at $f=100$ kHz; (a) $m=0.105$, (b) $m=0.110$.

Poincaré map. In this way any two points lying in the same piece and with coordinates differing by a very small amount, will be mapped after four periods in the other two close-lying points of that piece. The exponential divergence of the trajectories can be measured in terms of the Lyapunov exponent of the map[7] defined on that piece. One may observe parabolalike maps [Fig. 6(a)] until a crisis in the system appears. This crisis of the attractor is of the merging type since the four chaotic pieces are no longer visited regularly. After the merging, the attractor is composed of two bigger pieces which in turn are visited regularly.[10,12] The corresponding return maps [shown in Fig. 6(b) for $m=0.110$ and $f=100$ kHz] may still be described as effective one-dimensional maps which, however, have two extrema. This crisis occurs since the attractor touches the stable manifold of a saddle point generated in the process of saddle–node bifurcation as we change m.[9]

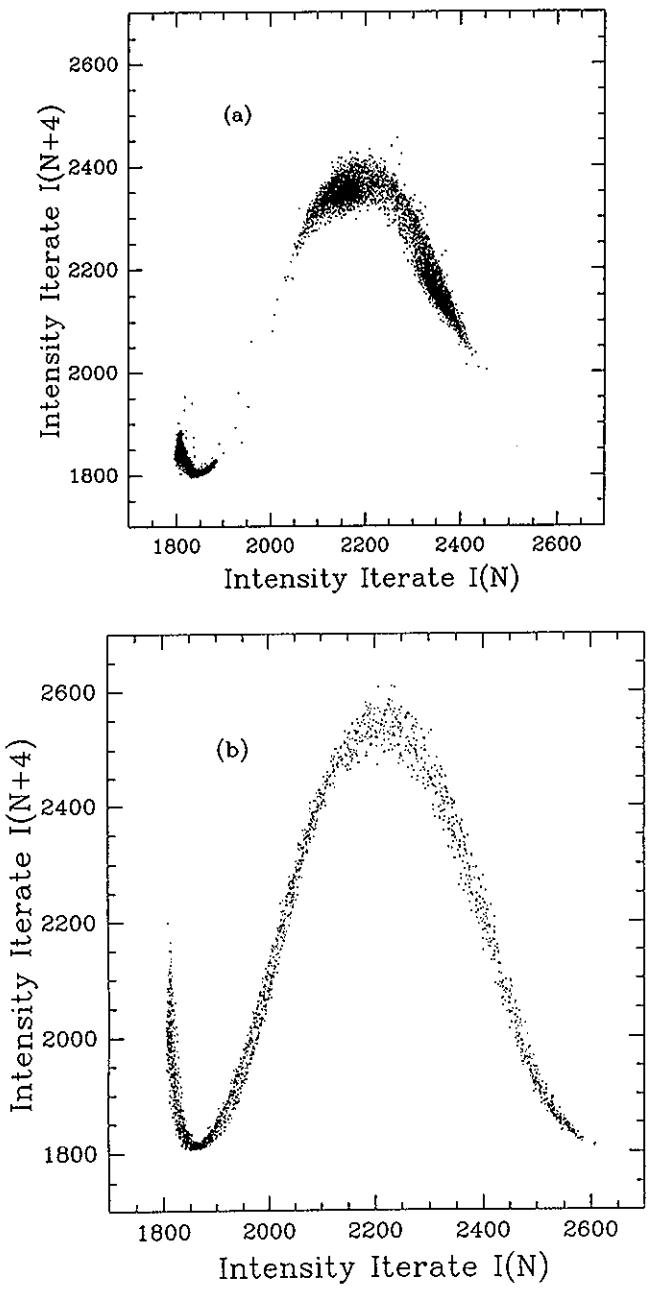

FIG. 7. Experimental return maps for the laser intensity obtained with the fourth iterates at $f=100$ kHz. (a) $m=0.118$, (b) $m=0.124$.

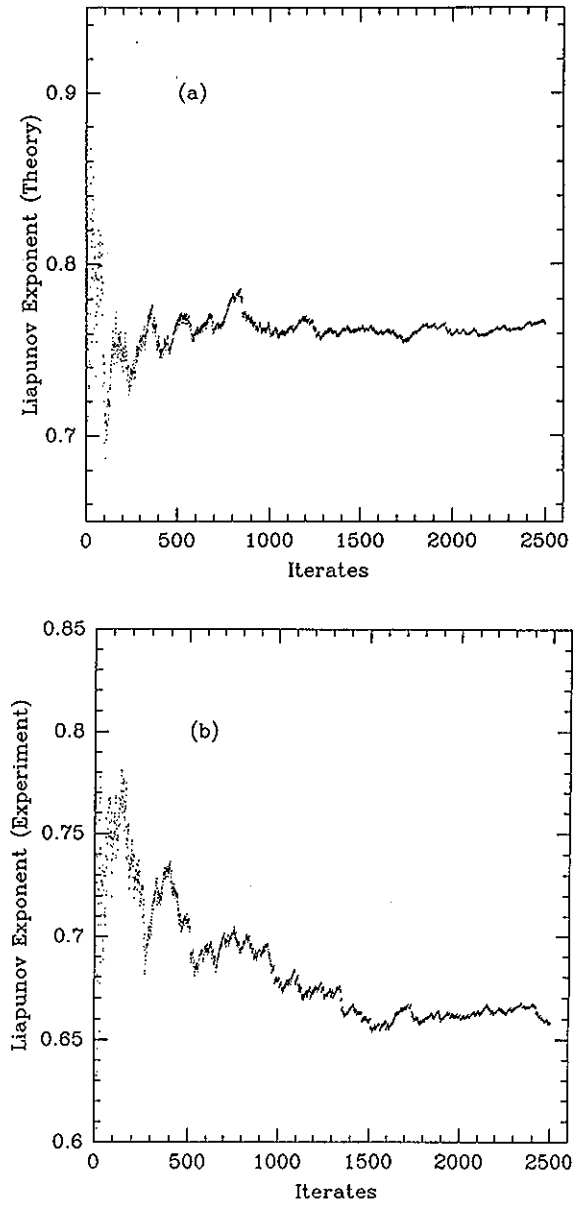

FIG. 8. Lyapunov exponents calculations for (a) the return map of Fig. 6(b) (λ_{th}) and (b) the return map of Fig. 7(b) (λ_{ex}).

In Figs. 7(a) and 7(b) we report the experimental return maps corresponding to Figs. 6(a) and 6(b), respectively. As in the experiment we observe only maps with two extrema, we argue that the attractor shown in Fig. 7(a) is sensitive to the experimental noise which induces a merging of the two attractor pieces. After the merging, however, the attractor is more stable against noise [Fig. 7(b)].

We can now evaluate the Lyapunov exponent of the return maps reported in Figs. 6(b) and 7(b) by fitting the theoretical and the experimental data with two polynomial curves $G(x)_{th}$ and $G(x)_{ex}$, respectively. The Lyapunov exponents of the maps are defined as follows:[7]

$$\lambda_{th(ex)} = \lim_{N\to\infty} \frac{1}{N} \sum_{i}^{N} \ln|G'(x_i)_{th(ex)}|.$$

Here N is the number of data points ($N=2500$). The evolutions of the Lyapunov exponents λ_{th} and λ_{ex} versus the number of data points are shown in Figs. 8(a) and 8(b), respectively. The numerical values, evaluated by averaging over the last 500 data points, are $\lambda_{th}=0.762$ and $\lambda_{ex}=0.662$ with the same standard deviation $\sigma=2.3\times10^{-3}$. The correlation dimension calculations performed on the theoretical and experimental Poincaré sections confirm the low dimensionality of the attractor, giving values a few percent above one.

IV. CONCLUSIONS

In the present paper we have shown that the four-level model is the only acceptable model to describe the chaotic behavior induced by loss modulation in a single mode CO_2 laser.

We have also established that for 4LM the period-bubbling behavior persists beyond the values of the modulation parameters for the onset of chaos until crises arise. In 2LMS, even for values of m lower than those of 4LM, crises arise already in the periodic regime. In this way crises, which in turn are related to multistability, destroy period bubbling. In contrast, period bubbling is allowed in 2LME.

The treatment of the dynamics in terms of one-dimensional maps has been possible, since just at the onset of chaos (reached by period doublings) any multidimensional system may be described as a noninvertible one-dimensional map, and since period bubbling is an indication of low dimensionality. The theoretical analysis of the Poincaré maps shows the transition from maps with one extremum to maps with two extrema, as a consequence of a merging-type crisis. Beyond the crisis, we find a fair agreement between the Lyapunov exponents calculated from the experimental and the numerical one-dimensional maps.

ACKNOWLEDGMENTS

This work was partly supported by the E.C. Contract No. SCI*-CT91-0697 (TSTS). C.L.P.L. is grateful for the hospitality of the Condensed Matter Group and Professor H. Cerdeira at the International Center of Theoretical Physics (Trieste, Italy). The authors also thank Professor G. Denardo for encouraging this work.

[1] F. T. Arecchi, R. Meucci, G. Puccioni, and J. Tredicce, Phys. Rev. Lett. **49**, 1217 (1982); G. Puccioni, A. Poggi, W. Gadomski, J. Tredicce, and F. T. Arecchi, *ibid.* **55**, 339 (1985); J. R. Tredicce, F. T. Arecchi, G. P. Puccioni, A. Poggi, and W. Gadomski, Phys. Rev. A **34**, 2073 (1986).

[2] J. Duprè, F. Meyer, and C. Meyer, Rev. Phys. Appl. (Paris) **10**, 285 (1975); E. Arimondo, F. Casagrande, L. A. Lugiato, and P. Glorieux, Appl. Phys. B **30**, 57 (1983); M. L. Asquini and F. Casagrande, Nuovo Cimento D **2**, 917 (1983).

[3] F. T. Arecchi, W. Gadomski, R. Meucci, and J. R. Roversi, Opt. Commun. **65**, 47 (1988); G.-L. Oppo, J. R. Tredicce, and L. M. Narducci, *ibid.* **69**, 393 (1989).

[4] V. Zehnle, D. Dangoisse, and P. Glorieux, Opt. Commun. **90**, 99 (1992).

[5] R. Meucci, M. Ciofini, and P. Wang, Opt. Commun. **91**, 444 (1992).

[6] G.-L. Oppo and A. Politi, Phys. Rev. A **30**, 435 (1984); M. Bier and T. C. Bountis, Phys. Lett. A **104**, 239 (1984); C. Lepers, J. Legrand, and P. Glorieux, Phys. Rev. A **43**, 2573 (1991).

[7] A. J. Lichtenberg and M. A. Lieberman, *Regular and Stochastic Motion* (Springer-Verlag, Berlin, 1983).

[8] E. Knobloch and N. O. Weiss, Physica D **9**, 379 (1983); W. Krolikowski, M. R. Belic, M. Cronin-Golomb, and A. Bledowski, J. Opt. Soc. B **7**, 1204 (1990).

[9] J. M. T. Thompson and H. B. Steward, *Nonlinear Dynamics and Chaos* (Wiley, New York, 1986).

[10] C. Grebogi, E. Ott, and J. A. Yorke, Physica D **7**, 181 (1983); Phys. Rev. Lett. **57**, 1284 (1986).

[11] D. Hennequin, P. Glorieux, and D. Dangoisse, Phys. Rev. Lett. **57**, 2657 (1986); H. G. Solari, E. Eschenazi, R. Gilmore, and J. R. Tredicce, Opt. Commun. **64**, 49 (1987); R. Meucci, A. Poggi, F. T. Arecchi, and J. R. Treddice, *ibid.* **65**, 151 (1988).

[12] C. Grebogi, E. Ott, F. Romeiras, and J. Yorke, Phys. Rev. A **36**, 5365 (1987).